Hindawi
Geofluids
Volume 2021, Article ID 5527299, 18 pages
https://doi.org/10.1155/2021/5527299

Research Article

Minerals Filling in Anhydrite Dissolution Pores and Their Origins in the Ordovician Majiagou Formation of the Southeastern Ordos Basin, China

Lihong Liu,[1,2] **Chunlian Wang**,[3] **Zhili Du**,[1] **and Jianghua Gong**[3]

[1]*Oil & Gas Survey, China Geological Survey, Beijing 100083, China*
[2]*Oil and Gas Research Center, School of Earth and Space Sciences, Peking University, Beijing 100871, China*
[3]*MNR Key Laboratory of Metallogeny and Mineral Assessment, Institute of Mineral Resources, Chinese Academy of Geological Sciences, Beijing 100037, China*

Correspondence should be addressed to Chunlian Wang; wangchunlian312@163.com

Received 20 January 2021; Revised 11 March 2021; Accepted 20 March 2021; Published 20 April 2021

Academic Editor: Guo Xiang Chi

Copyright © 2021 Lihong Liu et al. This is an open access article distributed under the Creative Commons Attribution License, which permits unrestricted use, distribution, and reproduction in any medium, provided the original work is properly cited.

Mold pore cementation is the key factor constraining the reservoir property in the study area. The anhydrite dissolution pores in the Ordovician Majiagou Formation of southeastern Ordos Basin are commonly filled by minerals such as dolomite, calcite, pyrite, and quartz accounting for more than 90% of the total molds resulting in significant porosity volume reduction. The anhydrite dissolution pores in the Jingbian Gas Field in the middle east of the basin, however, are rarely filled by minerals with more than 30% molds, remaining open to become good reservoir space. Studies reveal that the calcite filling in anhydrite dissolution pores has a relatively negative $\delta^{18}O$ value (-15.58‰~-8.96‰ VPDB) and negative $\delta^{13}C$ value (-7.56‰~0.26‰ VPDB), which is interpreted to be caused by thermochemical sulfate reduction (TSR). The higher homogenization temperatures (140-234°C) and high salinity (19.13-23.18 wt.% NaCl equivalent) of the primary inclusions in calcite confirm the above interpretation. Dolomite is the second most abundant carbonate formed as by-product of TSR, which is promoted by the precipitation of calcite and resulted enriched in Mg^{2+}/Ca^{2+} ratio in the pore water. Pyrite forms by the reaction of H_2S released from TSR with the Fe^{2+} in the horizon, which is supported by its cubic habit and relatively high $\delta^{34}S$ value (10.50‰~24.00‰VCDT). Quartz with relatively high homogenization temperature (113-154°C) is considered to precipitate in low-pH solution from calcite and pyrite precipitation after TSR. The southeastern Ordos Basin is much lower than the Jingbian Gas Field in paleogeographic location, which is submerged in the sea water of marine phreatic environments for a long time when sea water flooded from the southeastern direction. TSR occurs due to calcium sulfate enriched in pore water resulting in the minerals of dolomite, calcite, pyrite, and quartz filling in the molds leading to the low porosity and permeability of the study area.

1. Introduction

The anhydrite nodule-bearing dolomite is widely distributed in the Ordovician Majiagou Formation of southeastern Ordos Basin. The anhydrite nodule normally occurs in settings interpreted to be sabkhas [1, 2], intertidal to shallow subtidal [3], and even deeper subtidal settings [4]. The anhydrite nodules in the present case are formed in evaporative tidal flat facies but mostly leached by fresh water [5]. The nodular morphology suggests precursor gypsum or anhydrite. The gypsum is commonly dehydrated to anhydrite in the shallow burial condition; therefore, the nodules are normally filled by anhydrite when deep buried. Nevertheless, the anhydrite has been dissolved by fresh water during an episode of subaerial exposure during the Caledonian orogeny [6] forming the major reservoir space of the basin in the Ordos Basin. However, the anhydrite dissolution pores are commonly filled by minerals, such as dolomite, calcite, pyrite, and quartz, resulting in significant porosity and volume reduction. The minerals filling in molds are

conventionally interpreted to be formed in near surface conditions. However, the cementation of molds can occur at any time in the burial cycle from eogenesis through mesogenesis and into telogenesis.

The filling of anhydrite dissolution pores by calcite and dolomite can be interpreted as the replacement of sulfate by carbonate driven by various hydrological processes, such as bacterial sulfate reduction [7–9]. Pierre and Rouchy [7] interpreted the low $\delta^{13}C$ value from organic origin and the low $\delta^{18}O$ value caused by the large quantities of energy released during the bacterial sulfate reduction. It can also be the result of an active volcanogenic system [2] or even associated with cycling of seawater through hydrothermal anhydrite in mid-ocean ridges [10]. Late stage calcite replacement of evaporite nodules has also been reported to be associated with thermochemical sulfate reduction (TSR) [11, 12]. However, the most widely documented process is related to the meteoric water in the active phreatic zone but not in the deep subsurface [13–15]. The dissolution of sulfate and precipitation of minerals can significantly change the porosity and permeability of the horizon. To study the fabric and the formation process of replacement of evaporite is of economic and of scientific significance. Based on the outcrops and well cores in the southeastern Ordos Basin, thin section observation, stable isotopic analyses, scanning electron microscope (SEM), and fluid inclusion analyses are undertaken to study the time, process, and conditions of evaporite replacement to provide valuable information on the pore fluid properties and predict the reservoir quality.

2. Geological Background

The Ordos Basin, located in the middle-west of China, is the second largest basin in China with an area of 2.5×10^5 km^2 [16]. In the Ordovician Majiagou Formation, affected by the Helan Rift valley tension in the west of the basin, the rift shoulder rises forming the Central Uplift (also known as "L" shaped paleo-uplift group) [17–19]. Under the action of crustal equalization compensation, the compensating Shanbei Depression forms in the Middle East of the basin, which deposits anhydrite halite in drought-hot climate. The Jingbian Gas Field is located in the transitional zone between the Central Uplift and the Shanbei Depression (Figure 1). A set of dolomicrite to fine crystalline dolomite is developed in restricted to semirestricted platforms in the Jingbian Gas Field. The study area is located in the southeast of the basin far from the central uplift depositing anhydrite nodule-bearing dolomite in evaporite platform facies.

In the late Ordovician, the basin was uplifted and subjected to exposure for more than 140 My during Caledonian orogeny, forming a significant regional unconformity above the Majiagou Formation [6]. The Ordovician Majiagou Formation can be divided into six members. Member 6 is eroded in most regions and only found in the southern part of the basin with a thickness of 10 to 20 m. Members Ma_1 to Ma_5 are developed all over the basin and can be laterally traced for several kilometers. Owing to the periodic sea-level changes, a set of transgression–regressive cycles are deposited in the Majiagou Formation, in which Ma_1, Ma_3, and Ma_5 members are mainly composed of dolomite and anhydrite in evaporite platform facies, whereas the Ma_2, Ma_4, and Ma_6 members are dominated by limestone and dolomite in open platform facies (Figure 1) [16, 20]. Up to 10 submembers (Ma_5^1, Ma_5^2,…, Ma_5^{10}) have been identified in member 5 with cyclic carbonate-evaporite intervals related to the short term sea-level variations (Figure 1) [5]. The Ma_5^1 to Ma_5^4 submembers are mainly composed of fine microcrystalline dolomite, anhydrite, karst breccia, and anhydrite nodule-bearing dolomite. Because of the dissolution of anhydrite nodules in meteoric water, a favorable reservoir developed in the upper four submembers of the Ma_5 member, which became the major gas producing strata. Yican 1 well, drilled in 2014, produces 3.5×10^4 m^3 gas daily in Ma_5^1 and Ma_5^4 submembers where the anhydrite nodules, dolomite, and fractures are developed.

The anhydrite dissolution pores account for more than 90% of pore types both in the Jingbian Gas Field and the southeastern Ordos Basin. Mold pore cementation is the key factor constraining the reservoir property in the study area. The anhydrite dissolution pores in the Jingbian Gas Field are mostly filled by dolomite accounting for less than 70% of the total porosity with abundant pores remaining open, whereas the anhydrite dissolution pores of Yican 1 well are mainly filled by minerals accounting for more than 90% of the overall porosity in southeastern Ordos Basin, leading to the significant reduction of porosity (Figure 2) [21, 22]. Therefore, the porosity differences between the Jingbian Gas Field and the southeastern Ordos Basin are mainly caused by the filling degree of the anhydrite dissolution pores. Accurate analysis of the genesis of minerals filling in the pores is beneficial to understand the fluid activity process and predict effective reservoirs.

3. Samples and Methods

More than 60 samples from the Ordovician Majiagou Formation of Yican 1 well in the southeastern Ordos Basin over a depth of 2631 to 3132 m are examined by an optical microscope. Data from other wells of the Jingbian Gas Field were used for comparison.

Hand specimens of carbonates have been sampled selectively with a small drill to obtain samples from a very limited area. Samples used for carbon and oxygen analysis are mainly obtained from the gypsum molds and dolomite matrix. Powder samples (~30–50 mg per single sample) of limestone, dolostone, and anhydrite were extracted for carbon and oxygen isotope measurements. The powdered samples were heated to remove organic materials and then reacted with anhydrous phosphoric acid under vacuum to release CO_2 at 25°C for 24 h. The CO_2 was then analyzed for carbon and oxygen isotopes on a Finnigan MAT251 mass spectrometer. All carbon and oxygen data are reported in ‰ units relative to the Vienna Pee Dee Belemnite (VPDB) standard (Hoefs, 2009). The precision for both $\delta^{13}C$ and $\delta^{18}O$ measurements is better than ±0.1‰. Ultrafabrics were studied using a Melin-type scanning electron microscope (SEM) (Carl Zeiss AG) operated at 15–20 kV with a 10 nA beam curt and a working distance of 10 mm. The mineral composition was

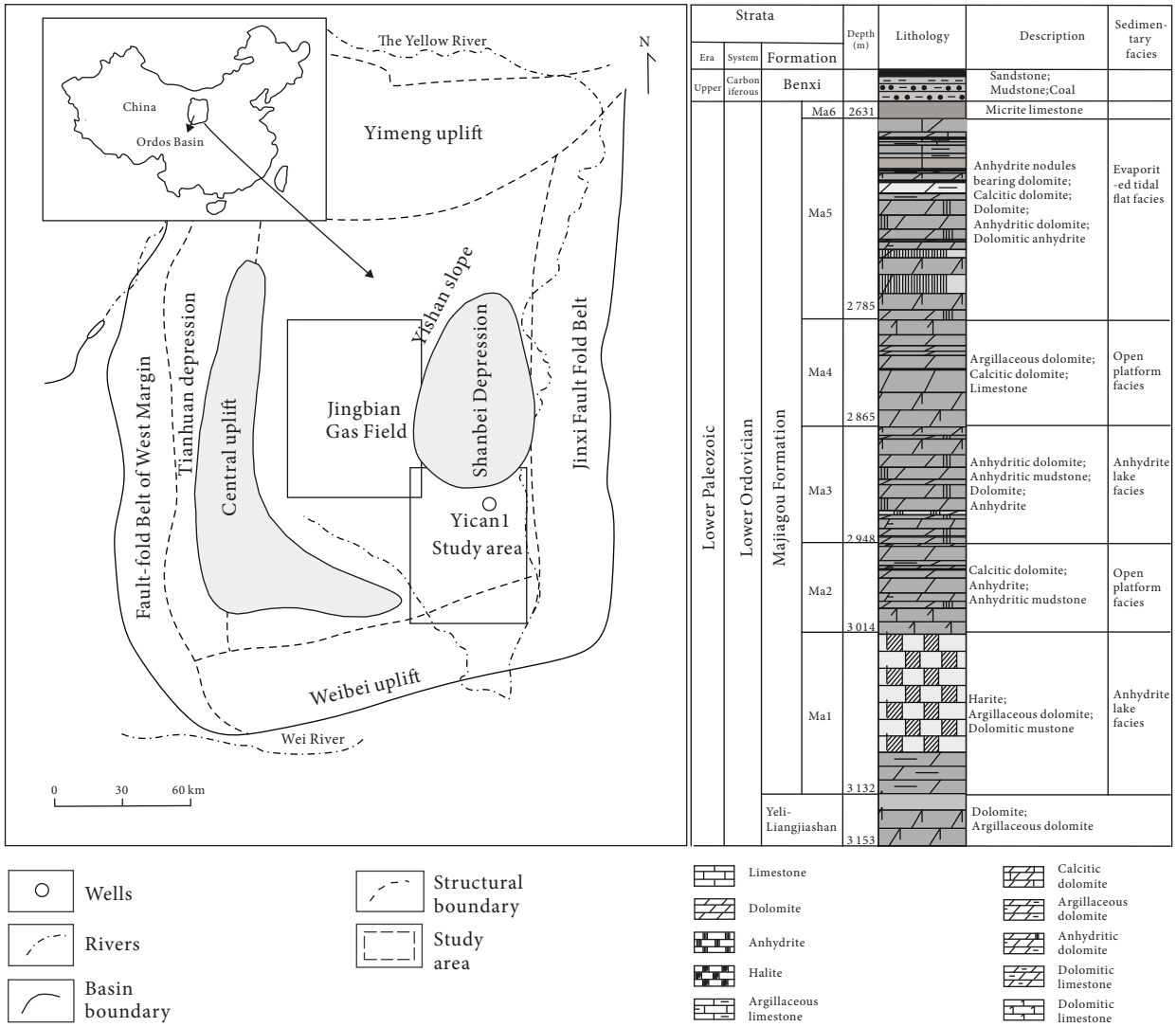

Figure 1: Simplified structural map of the Ordos Basin showing the study area and the Jingbian Gas Field [6] and the lithocolumn of the main sampled Yican 1 well.

observed by back scattered electron image (BSE), and the elemental concentrations and spatial variation of micron-sized spots were determined using energy-dispersive spectrometry (EDS) at the China University of Petroleum (College of Geosiences), which could generate high-resolution, high-magnification images revealing carbonate textures.

A total of 14 pyrite samples were analyzed for their sulfur isotope ratios. 30 mg of pyrite was mixed with Cu_2O at 1100°C under vacuum to produce SO_2. SO_2 was then analyzed on a Delta v plus Isotope Ratio Mass Spectrometer. The $\delta^{34}S$ values are reported relative to the Vienna-Canyon Biablo Troilite (V-CDT) standard [23]. The precision is better than 0.1‰.

Fluid inclusion heating-freezing analyses were conducted via a ZEISS Axioskop 40 A Pol with a Linkam THMS600 heating and cooling stages. An ultraviolet fluorescence system was used to discern hydrocarbon inclusions. The final melting temperature T_m and the homogenization temperature T_h were measured in all samples. Accuracy for measurements for homogenization temperature and melting temperature is ±1°C and ±0.1°C, respectively. The melting temperatures were converted to salinity values (equivalent wt.% NaCl) according to standard equations [23]. The bulk melting was close to the NaCl eutectic in most samples.

4. Results

4.1. Petrography. Anhydrite nodules primarily occur in thinly laminated dolomicrite, which also occur interlayered with anhydrite. The thinly laminated dolostones contain increasing amounts of anhydrite nodules from downward to upward of the unit. The nodules are spherical, ovoid, or, in some cases, elongate, ranging from 1 to 2 mm across (Figures 3(a)–3(d) and 4(a)–4(k)). Synsedimentary and early diagenetic nodular and contorted anhydrite structures are common diagnostic features of modern tidal environments [10]. The anhydrite nodules are partially or totally dissolved, where the carbonates display a vuggy internal

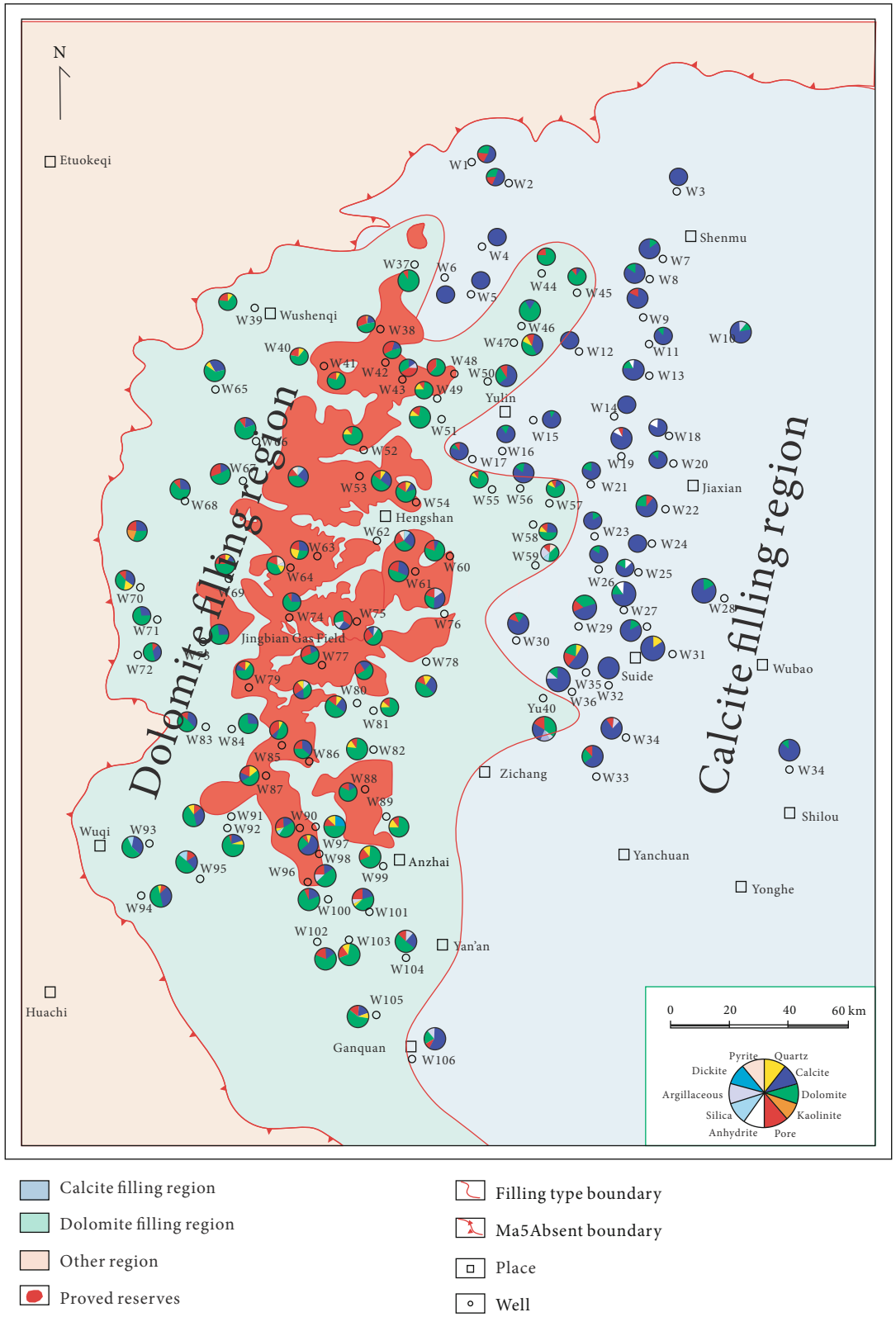

Figure 2: The distribution map of minerals filling in anhydrite dissolution pores in the Ordovician Majiagou Formation of Ordos Basin (modified from [21, 22]).

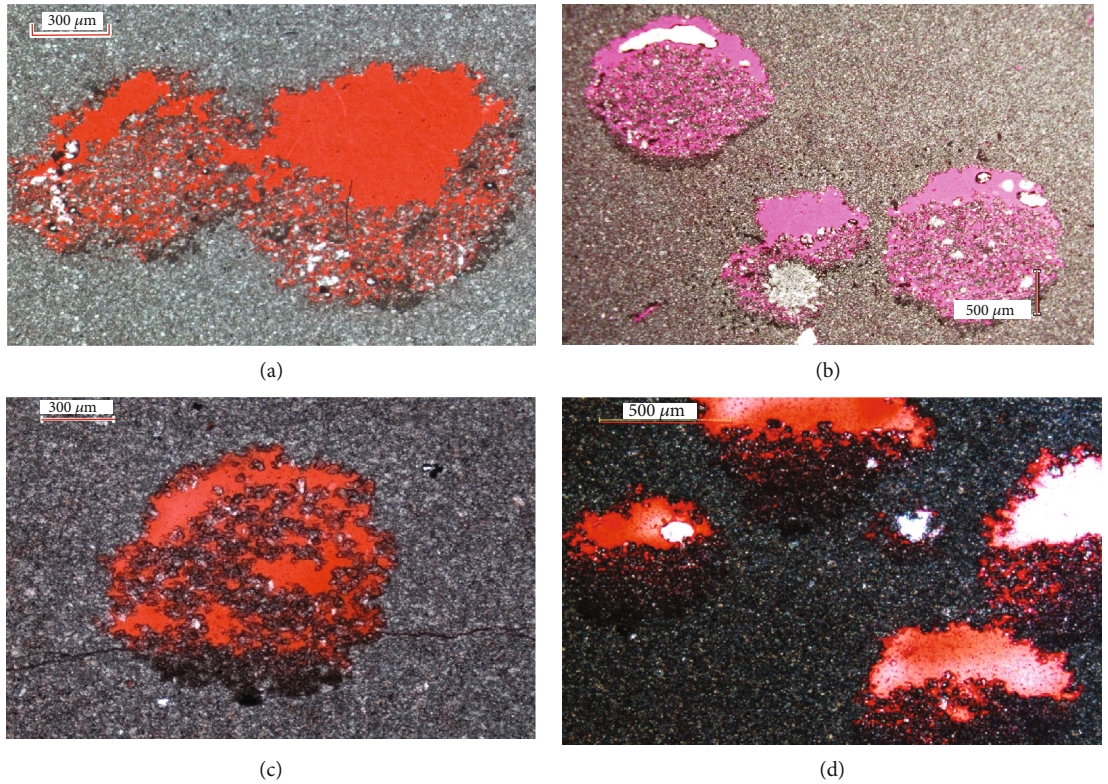

Figure 3: The occurring characteristics of anhydrite dissolution pores in the Ordovician Majiagou Formation in the Jingbian Gas Field (red and pink casting colors represent anhydrite dissolution pores).

microstructure, leaving molds to increase the overall reservoir properties. The anhydrite dissolution pores are more developed in the Jingbian Gas Field, which are rarely or partially filled by minerals (Figures 3(a)–3(d)). However, in the southeastern Ordos Basin, the molds are normally cemented by calcite, dolomite, quartz, etc. which resulted in the significant reduction of primary porosity in some core intervals.

4.1.1. Dolomite. Two types of dolomites are identified in the anhydrite dissolution pores. The first type is the fine crystalline dolomite at the bottom of the nodules (Figures 3(a)–3(d) and 4(c)–4(j)). The dolomite crystals at the bottom of the nodule are larger than the matrix dolomite with sizes ranging from 0.01 to 0.04 mm. The crystal density decreases, and the size increases from the bottom of the nodule towards the center of the mold. The fine crystalline dolomites are always at the bottom of the nodule as "seepage silts" forming the geopetal structures indicating the top of the horizon. The fine crystalline dolomite accounts for 60%-70% of the total nodule with the remaining pores open (Figures 3(a)–3(d)) or filled with other minerals (Figures 4(a)–4(k)). The pores are mainly filled with this type of dolomite in the Jingbian Gas Field with the remaining pores open (Figure 2). The remained pores account for 20%-30% of the nodule forming the major reservoir space of the unit.

The other type of dolomite occurs as euhedral dolomite crystals in the upper part of the nodules with crystal sizes in the range of 50-500 μm (Figures 4(c)–4(e)). The crystals are in rhombic morphology with cloudy surface. Fluorescent light images show that the hydrocarbon inclusions are abundant in the pores of seepage silt at the bottom of the nodule, and some are observed in the lattice defect of dolomite crystals (Figure 4(f)). Some dolomite crystals have slightly curved crystals with undulose extinction as saddle dolomites (Figure 4(g)).

4.1.2. Calcite. Different from the concentric structure defined by a succession of different types of quartz and carbonate phases documented in many literatures [10, 24], the nodules in this study are commonly composed of "seepage silt" at the bottom and carbonate phases and quartz at the top. The molds are formed by the dissolution of anhydrite and filled with blocky calcite spar (Figures 4(h)–4(j)). The calcite crystal morphology is outlined by the outer envelopes of the pore space. Individual crystal is normally coarse to very coarse crystalline of about 500-1000 μm in diameter. Some crystals are clear with crossed twinning apparently free of evaporite inclusions (Figure 4(h)). Many of the calcites contain primary hydrocarbon inclusions as shown in fluorescent light images (Figure 4(k)).

4.1.3. Quartz. The quartz is observed to fill the same pore or vug with calcite in direct contact with the long axes commonly perpendicular to the surface in which they lie as a single euhedral crystal (Figures 4(d) and 4(h)). The crystals are clear with few inclusions, which display unit or undulose extinction. The single euhedral crystal is mainly hexagonal, bipyramidal, and up to 0.5 mm long. SEM photos show the

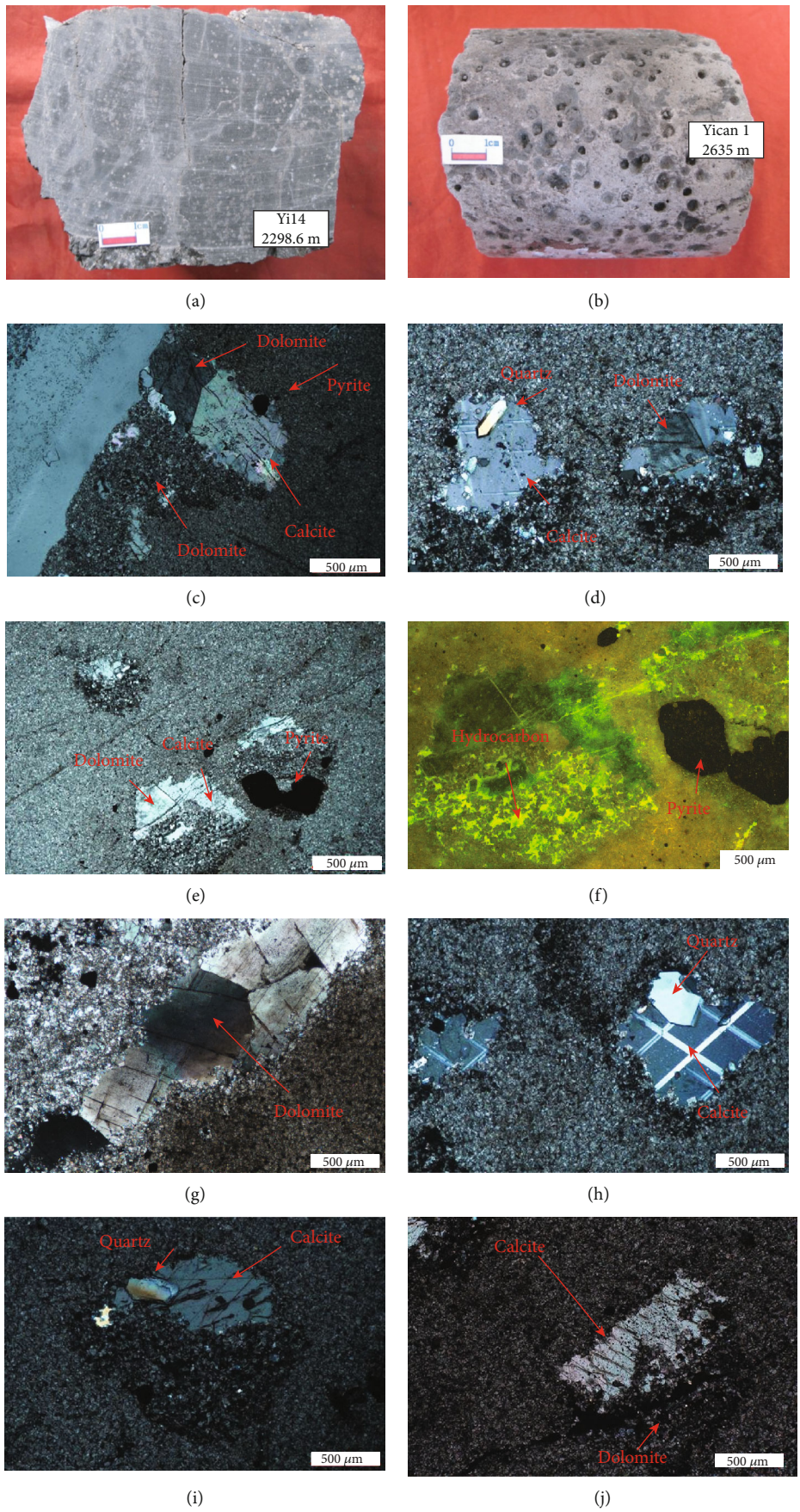

Figure 4: Continued.

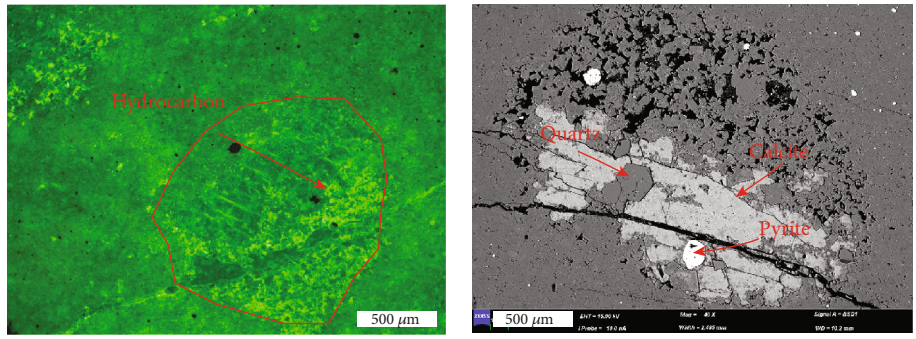

(k) (l)

Figure 4: Minerals filling in anhydrite dissolution pores of the Ordovician carbonate in Yican 1 well in the southeastern Ordos Basin. (a) Anhydrite nodule-bearing dolomite in Yi14 well, 2298.6 m, Ma_5^1. (b) Anhydrite dissolution pores in the core of Yican 1 well, 2635 m, Ma_5^1. (c) Anhydrite dissolution pores filled with dolomite, calcite, and pyrite in Yican 1 well, 2642.5 m, Ma_5^1, sample 96. (d) Anhydrite dissolution pores filled with dolomite, calcite, and quartz, 2641.4 m, Ma_5^1, sample 92. (e) Anhydrite dissolution pores filled with dolomite, calcite, and pyrite, 2642.5 m, Ma_5^1, sample 96. (f) Ultraviolet fluorescence photo shows hydrocarbon inclusions enriched in dolomite at the bottom of the nodule and lattice defect of calcite at the top of nodule, 2642.5 m, Ma_5^1, sample 96. (g) Saddle dolomite showing undulose extinction in the anhydrite dissolution pores, 2951.5 m, Ma_2, sample 242. (h) Calcite with crossed twinning and euhedral quartz filling in anhydrite dissolution pores, 2641.4 m, Ma_5^1, sample 92. (i) Anhydrite dissolution pores filled with calcite and quartz, 2642.5 m, Ma_5^1, sample 96. (j) Anhydrite dissolution pores filled with dolomite and calcite, 2640.9 m, Ma_5^1, sample 90. (k) Ultraviolet fluorescence photo shows hydrocarbon inclusions enriched in dolomite at the bottom of the nodule and lattice defect of calcite at the top of nodule, 2640.9 m, Ma_5^1, sample 90. (l) SEM photo of calcite, pyrite, and quartz filling in the anhydrite dissolution pores, 2641.4 m, Ma_5^1, sample 92.

high porosity in the fine crystalline dolomite at the bottom of the mold and the euhedral pyrite and quartz together with individual calcite crystal filling in the mold pore (Figure 4(l)).

4.1.4. Pyrite. Pyrite occurs as cubic crystals up to millimeter size scattered in laminated dolomicrite or in some cases within anhydrite dissolution pores (Figures 4(c) and 4(e)). The occurrence of pyrite is often accompanied by anhydrite, indicating its close association with the anhydrite dissolution. Under transmitted light, the crystal displays black color. Under SEM, the pyrite is white with Fe and S spectra identified from the EDS image (Figure 5).

4.1.5. Anhydrite. Anhydrite is found in nodules in the subsurface cores far from unconformity but rarely observed in nodules near the unconformity, indicating that the carbonate near the unconformity has undergone considerable late stage leaching of evaporite, resulting in the development of significant secondary porosity.

4.2. Geochemistry Data. Stable isotope compositions are determined for calcite cement and matrix dolomite. The data are plotted in Figure 6. The calcite cements have stable isotope values of $\delta^{18}O$ from -15.58‰ to -8.96‰ VPDB, average -12.12‰VPDB, and $\delta^{13}C$ from -7.56‰~0.26‰ VPDB, average -4.66‰ VPDB. Matrix dolomite has $\delta^{18}O$ from -10.95‰ to -6.75‰VPDB, average -8.47‰VPDB, and $\delta^{13}C$ from -6.87‰ to 0.18‰ VPDB, average -1.84‰ VPDB. Sulfur isotope analysis result shows that the $\delta^{34}S$ value of pyrite is between 10.50‰ and 24.00‰ VCDT with an average 17.33‰ VCDT ($n = 11$).

4.3. Homogenization Temperature of Fluid Inclusions. The fluid inclusions in calcite have a varied size of 1-10 μm but are mostly smaller than 5 μm as single or groups (Figures 7(a)–7(c)). Some fluid inclusions are two-phase liquid-gas inclusions, which can be classified as primary and secondary inclusions. The primary inclusions occur as a single inclusion in the crystal or isolated away from other inclusions (Figure 7(c)). The fluid inclusion assemblage (FIA) concept has also been used in the study as they are cooccurrence of different types of inclusions of the same origin in the same host minerals [25]. An ultraviolet fluorescence system was used to discern hydrocarbon inclusions. Under the optical microscope, liquid hydrocarbon inclusions show light brown or straw yellow in transmission light, and the gas hydrocarbon inclusions are commonly brown colors (Figure 7(d)). Some gas hydrocarbon inclusions show brownish black color in transmission light (Figures 7(e) and 7(f)), whereas under ultraviolet fluorescence light, the hydrocarbon always shows fluorescence color from green (Figure 7(g)), strong yellow (Figures 7(h) and 7(i)), to weak blue and orange color with increasing thermal evolution degree.

The homogenization temperatures of the primary inclusions in calcite and dolomite are in between 140 and 234°C ($n = 6$) and 190 and 193°C ($n = 2$), respectively (Table 1). The NaCl-equivalent salinities range from about 19.13 to 23.18 weight % approaching halite saturation. The quartz filling in the anhydrite dissolution pores had similar fluid inclusion homogenization temperatures as the associated calcite cements in a range of 113-154°C with an average 131°C ($n = 4$).

4.4. The Total Salinity of Formation Water. The total salinity of formation water has been analyzed as listed in Table 2. The total salinity of the formation water of the Ordovician Majiagou Formation in the southeastern Ordos Basin is very high, which can be up to 295.04 g/L, an average 150.31 g/L. The water type is mainly $CaCl_2$. The high salinity of the formation water shows that the $CaSO_4$ concentration is very high as shown in Table 2.

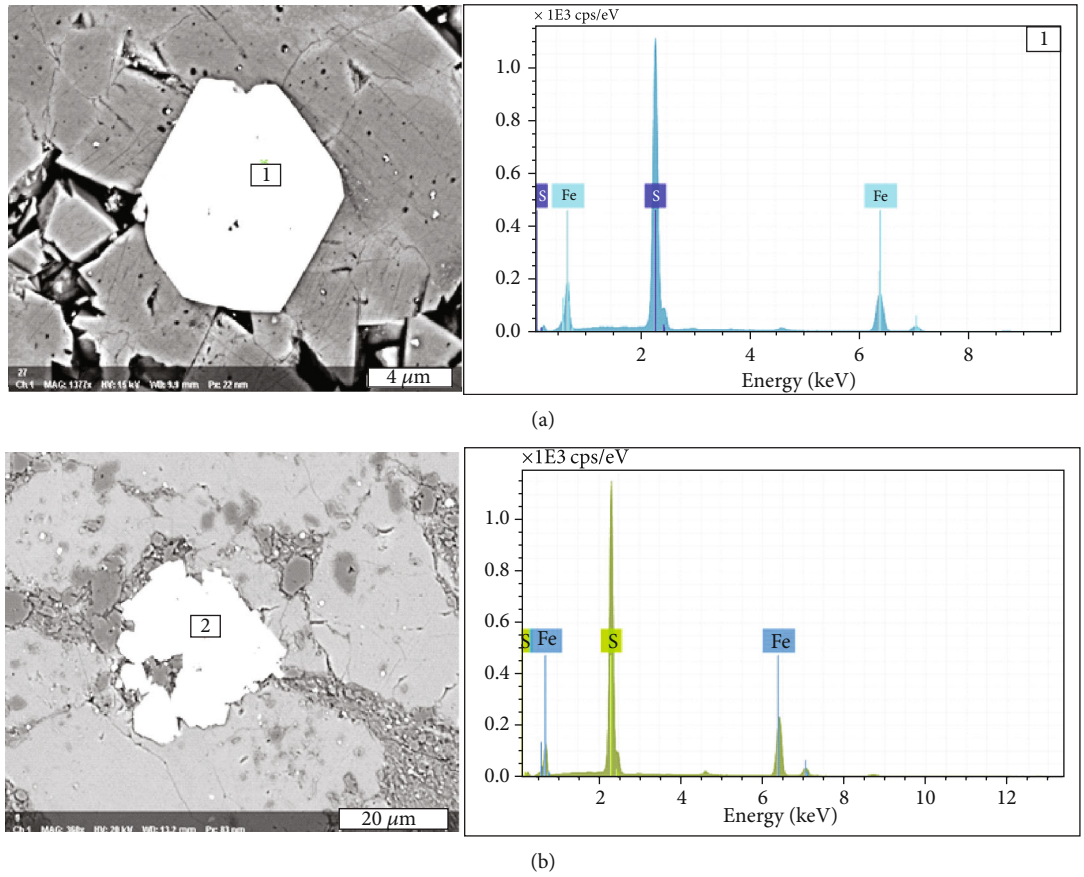

Figure 5: SEM and EDS analysis results of pyrite in Yican 1 well of the southeastern Ordos Basin. (a) Cubic pyrite in Yican 1 well, 2646.64 m, Ma_5^1. (b) Pyrite assemblage in Yican 1 well, 2684.86 m, Ma_5^4.

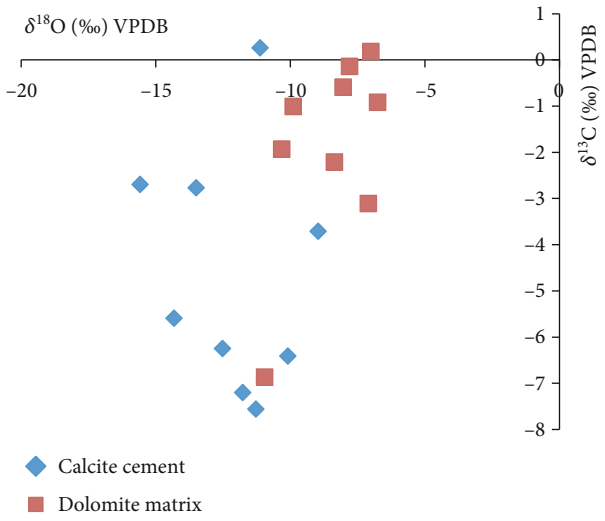

Figure 6: Cross-plot of $\delta^{18}O$ vs. $\delta^{13}C$ values of calcite cement and dolomite matrix of Yican 1 well in the southeastern Ordos Basin.

5. Discussions

Anhydrite nodule-bearing dolomite was interpreted to be formed by the penecontemporaneous dolomitization mode of the sabkha evaporative tidal flat [26]. The anhydrite and dolomite cyclical intervals are typical for shallow subtidal to supratidal evaporative settings. The dissolution molds are permeated by meteoric water during an episode of subaerial exposure during the Caledonian orogeny as they are restricted to the upmost 10 m below unconformity [6]. However, the cementation of the molds probably occurs in late burial settings.

5.1. Origin of Minerals Filling in Anhydrite Dissolution Pores

5.1.1. Calcite. The clean calcites containing no anhydrite inclusions suggest that they grow slowly in an open space where the anhydrite has been removed, which is confirmed by the existence of seepage silt at the bottom of the mold. The hydrocarbon inclusions in the calcite and in the residual pores at the bottom seepage silt indicate that the calcite probably precipitates when the hydrocarbon migrates to react with the dissolved sulfate in the pores. The original pore water in the Majiagou Formation would have been normal seawater to evaporative brines as the host rock consists of shallow marine platform limestone in the lower part of the formation and extensive evaporative facies in the upper part of the formation [27–29]. The initial pore fluid could have been diluted by meteoric water in much of the basin during the extended period of subaerial exposure [29]. The aqueous fluid inclusions in calcite filling in the molds, however, have

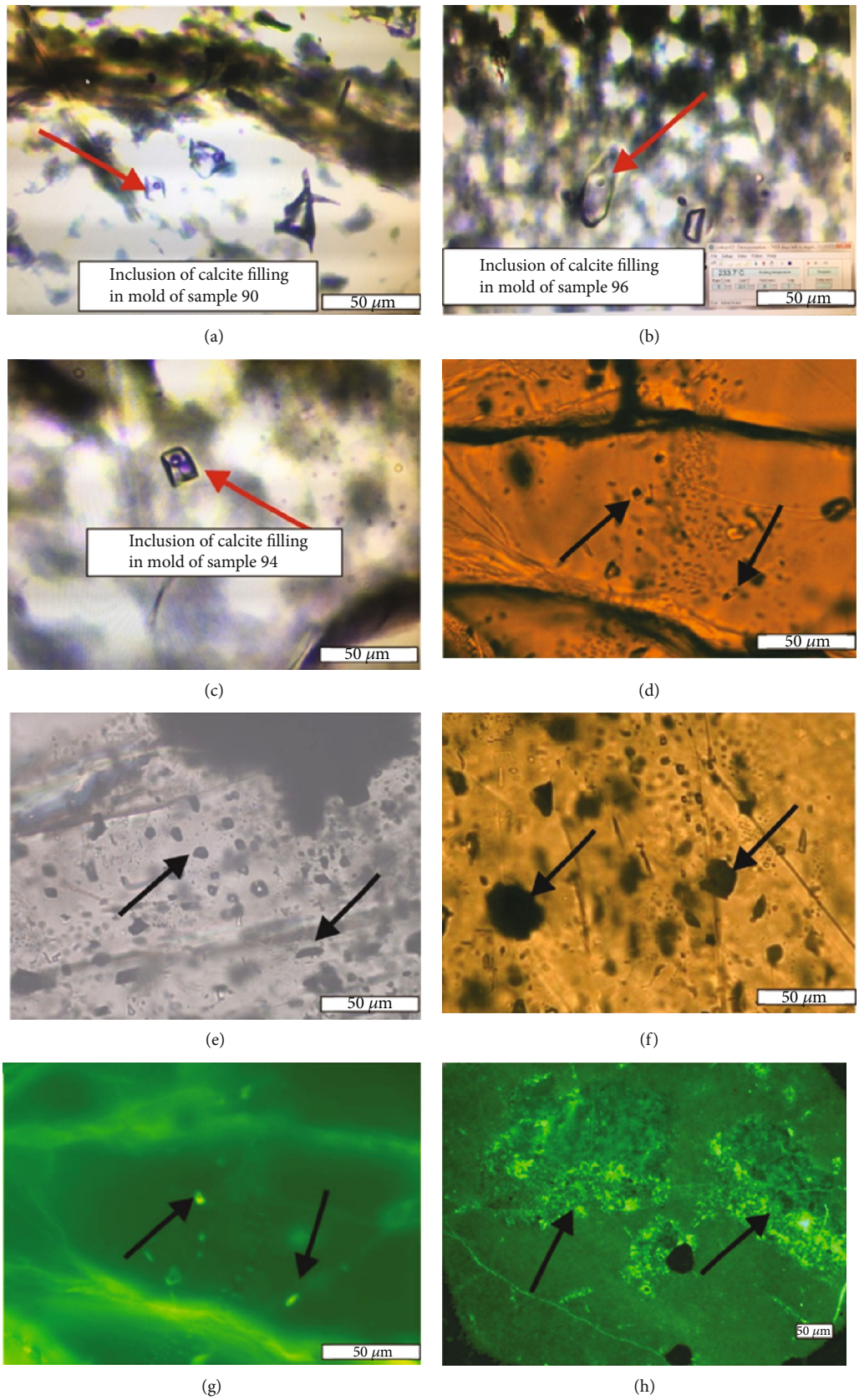

Figure 7: Continued.

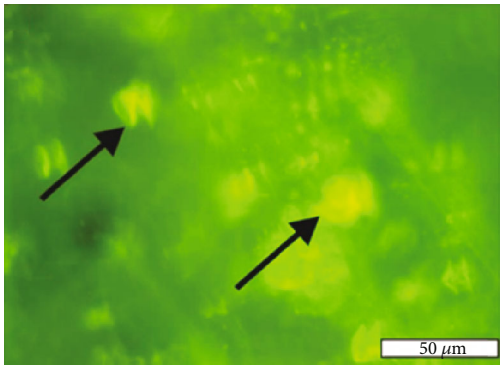

(i)

Figure 7: Characteristics of fluid inclusions in minerals filling in anhydrite dissolution pores in Yican 1. (a) Two-phase liquid-vaporous inclusions (WL+V) in calcite filling in anhydrite dissolution pores corresponding to Figures 4(j) and 4(k), 2640.9 m, Ma_5^1, sample 90. (b) Two-phase liquid-vaporous inclusions (WL+V) in calcite filling in anhydrite dissolution pores corresponding to Figure 4(i), 2642.5 m, sample 96. (c) Two-phase liquid-vaporous inclusions (WL+V) in calcite filling in anhydrite dissolution pores, 2641.8 m, sample 94. (d) Two-phase hydrocarbon inclusions of calcite filled in fracture showing light brown (OL) and black color (OV) in transmission light, 2642.5 m, sample 96. (e, f) Vaporous hydrocarbon inclusions (OV) of calcite showing black color in transmission light, 2635 m, sample 73. (g) Two-phase hydrocarbon inclusions of calcite filled in fracture showing light yellow (OV) and no fluorescence light (OV) in ultraviolet fluorescence light (the same thin section of (d)), 2642.5 m, sample 96. (h) Liquid hydrocarbon (OL) in the dolomite at the bottom of mold showing light green color in ultraviolet fluorescence light, 2641.8 m, sample 94. (i) Vaporous hydrocarbon inclusions (OV) of calcite showing yellow color in ultraviolet fluorescence light (the same thin section of (f)), 2635 m.

Table 1: Homogenization temperature of fluid inclusions in minerals filling in anhydrite dissolution pores in Yican 1 of the southeastern Ordos Basin.

No.	Samples	Minerals filling in molds	Homogenization temperature (°C)	Average (°C)	Melting temperature (°C)	Calculated salinity (%)	Average (%)
1	94	Dolomite	190	193	-17.3	20.45	21.81
2	94	Dolomite	196		-21.2	23.18	
3	90	Calcite	148	172	-15.6	19.13	21.03
4	90	Calcite	164		-15.6	19.13	
5	94	Calcite	174		-17.1	20.3	
6	94	Calcite	170		-18.4	21.26	
7	96	Calcite	140		-21.2	23.18	
8	96	Calcite	234		-21.2	23.18	
9	94	Quartz	113	131	-20.1	22.44	16.59
10	94	Quartz	129		-20.1	22.44	
11	96	Quartz	127		-18.7	21.47	
12	96	Quartz	154		10	0.02	

Table 2: Formation water composition of some wells of the Ordovician Majiagou Formation in the southeastern Ordos Basin.

Well	Formation	Section (m)	Ion content (mg/L)						Total salinity (g/L)	Water type
			K^++Na^+	Ca^{2+}	Mg^{2+}	Cl^-	HCO_3^-	SO_4^{2-}		
Yi 5	Ma_5^1	2317.0-2326.0	16749	79320	7660	180940	839	9529	295.04	$CaCl_2$
Yi 6	Ma_5^1	2295.0-2336.0	13522	66198	11951	167437	874	6556	266.54	$CaCl_2$
Yi 18	Ma_5^4	2358.0-2379.0	36382	10060	916	68225	530	10850	126.96	$CaCl_2$
Yi 8	Ma_5^1	2247.0-2257.0	17176	20623	3968	59278	204	20494	121.74	$CaCl_2$
Yi 14	Ma_5^1	2279.0-2300.0	9975	15090	1831	43619	394	4822	75.73	$CaCl_2$
Yi 12	Ma_5^1	1998.0-2034.5	2548	2347	610	8575	170	1607	15.86	$CaCl_2$

Table 3: Carbon and oxygen isotope results of calcite filling in mold and corresponding dolomite matrix in Yican 1 well in the southeastern Ordos Basin.

Samples	Depth (m)	Lithology	Formation	δ^{13}C of calcite in mold (VPDB ‰)	δ^{18}O of calcite in mold (VPDB ‰)	δ^{13}C of dolomite matrix (VPDB ‰)	δ^{18}O of dolomite matrix (VPDB ‰)
92	2641.38	Dolomicrite	Ma_5^1	0.26	-11.12	-0.59	-8.04
152	2688.00	Dolomicrite	Ma_5^4	-5.59	-14.32	-1.01	-9.89
164	2729.92	Dolomicrite	Ma_5^6	-7.56	-11.27	-6.87	-10.95
172	2731.80	Dolomicrite	Ma_5^6	-6.25	-12.52	-2.21	-8.36
186	2808.49	The fine crystalline dolomites	Ma_4	-2.70	-15.58	-1.93	-10.32
220	2821.06	The fine crystalline dolomites	Ma_4	-2.77	-13.49	-0.92	-6.75
228	2823.70	The fine crystalline dolomites	Ma_4	-7.20	-11.76	-0.14	-7.80
229	2823.80	The fine crystalline dolomites	Ma_4	-6.41	-10.09	0.18	-7.00
232	2945.62	The fine crystalline dolomites	Ma_3	-3.71	-8.96	-3.11	-7.10
Average				-4.66	-12.12	-1.84	-8.47

high T_h values (140-234°C) and high salinity (19.13-23.18 wt.% NaCl equivalent). The occurrence of fluids with salinities of higher than that of seawater (ca. 3.5 wt.%) is a direct indication of no influence of meteoric water. The exclusion of the involvement of meteoric water in spite of a substantial period of subaerial exposure suggests that the calcite filling in molds might have occurred after the subaerial exposure event and probably in the burial conditions. The homogenization temperature of calcite and dolomite is 140-174°C and 190-196°C, respectively, reflecting the deep burial diagenetic setting. The calcite filling in molds, therefore, is interpreted to have been precipitated from residual evaporative brine that had been locally preserved in the basin. Carbonate reservoirs with associated anhydrite, such as the anhydrite dissolution pores, are optimum sites for TSR, where the evaporative brines are remained in the pores.

This interpretation is further supported by the carbon and oxygen isotope composition of the calcite filling in the anhydrite dissolution pores. The presence of a possible hydrocarbons in the molds, together with its very low carbon isotopes (-7.56‰~0.26 VPDB) in calcite (Figure 6, Table 3) suggests that the calcite precipitation occurred in the presence of liquid hydrocarbons [30]. The oxygen isotope of calcite filling in anhydrite dissolution pores range from -15.58‰ to -8.96‰ VPDB, significantly negative to those in matrix dolomite, ranging from -10.96‰ to -6.75‰ VPDB (Figure 6, Table 3) indicating the effect of elevated temperatures, which drive the thermal fractionation of diagenetic carbonate [31–33]. The calcite, therefore, is most likely byproduct of TSR, where the hydrocarbon reacts with sulfate in residual pore water in high temperatures of deep burial condition. The porosity is lost due to the precipitation of authigenic calcite and dolomite.

The simplest TSR reaction can be written as [34]

$$nCaSO_4 + C_nH_{2n+2} \rightarrow nCaCO_3\ (\text{or } CO_2) + H_2S + (n-1)S + nH_2O. \quad (1)$$

The reaction provides the most reasonable explanation for both occurrences of authigenic calcite and oxidization of organic matter whose carbon is incorporated into the calcite [35, 36].

Although the lowest temperature for TSR is controversial, the available data indicate that as a generalization, the minimum temperature range of TSR is about 100-140°C [37]. Hence, in most geological settings, TSR occurs as soon as the temperature reaches this range, provided the necessary "ingredients" (sulfate, reactive organics, and some sulfur in a reduced form) are present [38]. Since uplifting and erosion in Caledonian, the Ordovician stratum is buried continuously until the late Cretaceous [39]) (Figure 8). Using geothermal gradients of 36°C/km and a surface temperature of 20°C, the temperature of 100°C reflects a depth of about 2200 m in early Triassic. TSR can proceed from 2200 m to the maximum depth of about 5000 m in late Cretaceous.

5.1.2. Dolomite. The fine crystalline dolomite at the bottom of the nodules is commonly interpreted to be formed by the dissolution of anhydrite and the reprecipitation of dolomite solute as "seepage silt." The composition of this dolomite, therefore, is the same as the matrix dolomite, whereas the

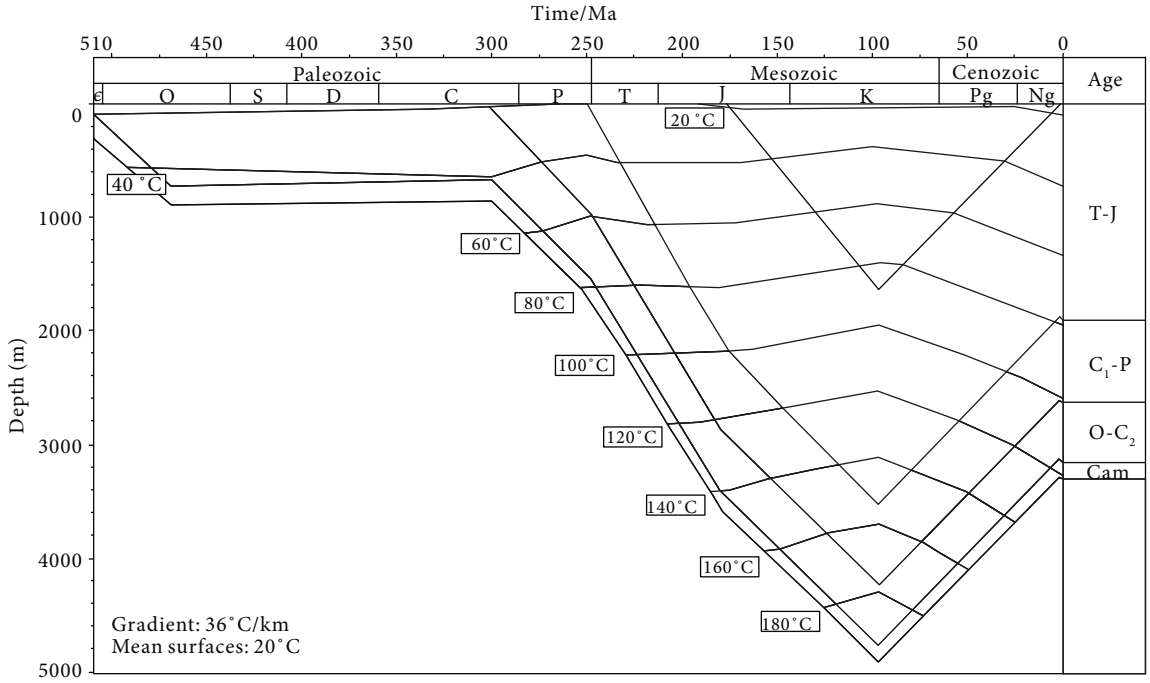

Figure 8: The burial history diagram of Yican 1 in the southeastern Ordos Basin (modified from [39]).

crystal size is commonly larger than that of matrix. The occurrence of seepage silts is a typical characteristic of meteoric water flushing in epigenetic stage.

The milky white, medium to coarse crystalline saddle dolomites in anhydrite dissolution pores are probably TSR dolomite. The abundant hydrocarbons in the pores of seepage silt at the bottom of the mold and in the lattice defect of dolomite crystals indicate simultaneously migration of hydrocarbons with the formation of crystalline dolomite. Saddle dolomite with undulose extinction is the typical characteristic of hydrothermal effect [33, 40], which is confirmed by its high homogenization temperature up to 193°C. Dolomite is the second most abundant carbonate formed as byproduct of TSR. TSR dolomite is almost exclusively restricted to the anhydrite-bearing dolomite associated with TSR calcite. Pressure solution is considered the chief source of Mg^{2+} for TSR dolomite [37]. The precipitation of calcite increases the Mg^{2+}/Ca^{2+} ratio in the pore water, which also promotes the dolomitization.

5.1.3. Pyrite. Pyrite is pervasively observed to occur as cubic, euhedral crystal (10-1000 μm) at the bottom of the mold or surrounding it. The cubic habit of pyrite (and the absence of framboidal pyrite) may indicate a nonbacterial origin with a relatively slow crystal growth rate during burial diagenesis at elevated temperatures.

Pyrite can be formed by the reaction of Fe^{2+} with S^{2-} as soon as in contact. S^{2-} can be originated from deep magma in volcanism [41], desulfurization of organic matter [42], bacterial sulfate reduction (BSR) [43, 44], or TSR. Previous studies reveal that the $\delta^{34}S$ of deep magma ranges from -5.6‰ to 5.5‰ [45]. The Ordos Basin is a stable cratonic basin, which excludes the possibility of volcanism. The pyrite formed by BSR commonly has a negative $\delta^{34}S$ value with an average from -42.7‰ to -5‰ [46, 47]. BSR is known from a multitude of geological settings that range in temperature from 0 to about 80°C [48, 49]. The homogenization temperature of fluid inclusions in calcite is between 140 and 234°C, in which the sulfate reduction bacteria cease to metabolize. The $\delta^{34}S$ value of TSR pyrite is commonly positive, which is reported to be from 8.9‰ to 23.4‰ of the pyrite from the Dengying Formation in Sichuan Basin [50] and 30‰ to 33‰ from the Upper Cambrian [36]. The pyrite in this study has a range of $\delta^{34}S$ from 10.50‰ to 24.00‰ with average 17.33‰ ($n = 11$), which can only be obtained from TSR.

H_2S is the most convincing and commonly known byproduct of TSR [51, 52]. However, the H_2S concentration is very low in Yican 1 well, which is only observed at 2823.7 m with low concentration. The most important reason for the widespread of pyrite and scarcity of H_2S is due to the presence of significant amount of Fe^{2+} in the horizon ($3387.5 \times 10^{-6} - 23112.5 \times 10^{-6}$) (Table 4). H_2S released from TSR is initially dissolved in the formation water in H^+ and S_2^{2-} form (Reactions (2) and (3)). The later will react with Fe^{2+} within seconds to minutes to form metal sulfides (Reaction (4)). H_2S is effectively removed as metal sulfide precipitation almost instantaneously, as soon and as long as base metals are available [38]. The Fe^{2+} content can be up to 23112.5×10^{-6} (Table 4) at the H_2S produced site of Yican 1 well, which abundantly assumed the H_2S released from TSR. The reaction between Fe^{2+} and H_2S reduces the concentration of H_2S and increases the pervasively occurrence of pyrite.

$$H_2S(aq) \rightarrow H^+ + HS^-, \quad (2)$$

$$2HS^- \rightarrow 2H^+ + S_{2-}^2, \quad (3)$$

Table 4: Geochemistry data of pyrite from Yican 1 in the southeastern Ordos Basin.

Samples	Depth (m)	Formation	Lithology	Pyrite $\delta^{34}S$ (VCDT, ‰)	Matrix $\delta^{13}C$ (VPDB, ‰)	Matrix $\delta^{18}O$ (VPDB,‰)	Matrix Fe × 10^{-6}	Matrix Mn × 10^{-6}
71	2634.7	Ma_5^1	Dolomicrite	11.90	/	/	/	/
72	2634.9	Ma_5^1	Dolomicrite	18.80	/	/	/	/
83	2637.4	Ma_5^1	Micrite limestone	11.10	-10.28	-10.62	15200.00	115.72
85	2638.7	Ma_5^1	Micrite limestone	20.00	-4.39	-10.44	8362.50	156.48
108	2646.6	Ma_5^1	Micrite limestone	-7.6	-1.44	-9.77	8312.50	224.88
122	2677.5	Ma_5^4	Dolomicrite	10.50	-0.86	-8.69	13950.00	99.42
249	2954.5	Ma_2	The fine crystalline dolomites	15.10	-0.46	-8.74	3387.50	85.24
308	3122.2	Ma_1	Dolomicrite	24.00	-3.25	-7.84	17450.00	139.44
314	3123.8	Ma_1	Dolomicrite	22.90	-3.92	-8.07	19412.50	257.64
320	3125.8	Ma_1	Dolomicrite	19.00	-4.90	-8.02	23112.50	258.48
321	3126.2	Ma_1	Dolomicrite	17.00	/	/	/	/
329	3128.76	Ma_1	Dolomicrite	20.30	-0.90	-7.50	9912.50	410.52

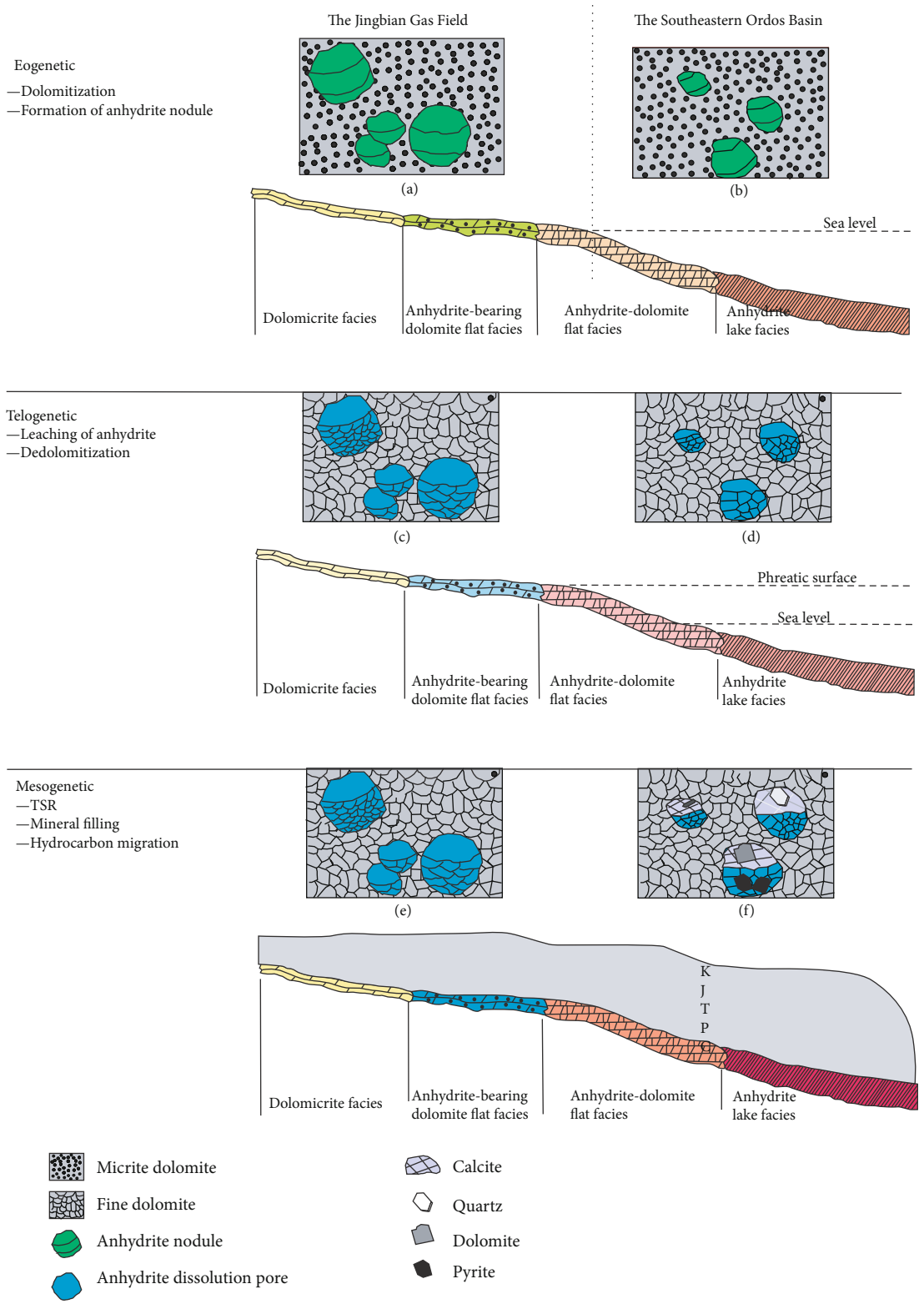

Figure 9: Diagenetic evolution comparison of minerals filling in anhydrite dissolution pores in the Ordovician Majiagou Formation of the southeastern Ordos Basin and the Jingbian Gas Field.

$$Fe^{2+} + S_{2-}^{2} \rightarrow FeS_2(pyrite). \quad (4)$$

5.1.4. Quartz. The silicification of evaporite is commonly thought to occur prior to significant burial (less than 500 m) [11]. Quartz is conventionally interpreted to be precipitated from solutions with higher silica concentrations from the dissolution of clastic quartz and other silicates of the mudstones or surrounding detrital deposits. The

dissolution and replacement of anhydrite by quartz, therefore, are indicative of the circulation of groundwater supersaturated in silica [24]. In the present case, the lack of anhydrite inclusions in quartz indicates that the quartz postdates the dissolution of anhydrite. The euhedral morphology of the quartz suggests that the quartz grows in sufficient space, where the anhydrite had probably been removed to form central hollows that later allows the euhedral crystals to grow. The relatively high homogenization temperature of fluid inclusions in quartz (113-154°C) strongly suggests that they are formed in deep burial conditions, which is probably related to TSR. Quartz is considered kinetically favorable to precipitate from low-pH solution [53–55]. H^+ released from calcite (Reaction (1)) and pyrite precipitation (Reaction (2) and (3)) is expected to locally decrease the pH value of the formation water, which is favorable for the precipitation of authigenic quartz. This can give a good explanation for the close temporal and spatial association of calcite and quartz [55]. In the present case, the authigenic quartz filling in anhydrite mold is, therefore, formed as a burial diagenetic process instead of an early diagenetic process.

5.2. Diagenesis Evolution and Comparison with the Jingbian Gas Field. The paleogeographic location of the southeastern Ordos Basin is much lower than that of the Jingbian Gas Field [56]. The sedimentary environment of the Jingbian Gas Field is mainly dolomicrite flat subfacies and anhydrite-bearing dolomite flat subfacies of the supratidal zone, whereas the southeastern Ordos Basin is mainly located in anhydrite-dolomite flat subfacies and anhydrite lake subfacies of intertidal zone (Figure 9). When the sea level decreases, the anhydrite nodules begin to form in the Jingbian Gas Field of supratidal zone. For longer evaporative time, the anhydrite nodules are more abundant, and the nodule size is larger in the Jingbian Gas Field (Figure 3, Figures 9(a) and 9(b)).

When uplifted in Caledonian orogeny in late Ordovician, the horizon experienced the leaching of meteoric water resulting in the anhydrite nodules dissolved, leaving the molds enriched in anhydrite dissolution water (Figures 9(c) and 9(d)). With the sea level increasing in Carboniferous-Permian, the southeastern Ordos Basin is flooded by the ocean from the south and east direction subsequently [22]. The formation is submerged in sea water of marine phreatic environments for a long time, leading to the pore water enriched in marine water. Owing to the periodic sea-level changes, the connate marine pore water is altered locally by minor amounts of evaporative water during shallow burial resulted in the pore water enriched in calcium sulfate (Table 2). Most minerals are preferentially hydrophilic so that a film of residual water lines the grain framework even in hydrocarbon gas-bearing reservoirs [57]. The amount of this residual water is generally ~10% of the pore volume of the rock. Reactions occurring in solution are generally many orders of magnitude faster than reactions between gases and solids [58]. Therefore, the hydrocarbons reacted with the dissolved anhydrite in solution in the residual water film rather than as a solid-gas reaction [34]. Since being uplifted in the Caledonian orogeny in the late Ordovician of the lower Paleozoic, the Ordos Basin experienced continuous burial until the deepest burial in the early Cretaceous, as shown in previous studies (Figure 8) [39]. The burial temperature has been above the minimum temperature of about 100°C in 2200 m of the early Triassic (using 36°C/km as a geothermal gradient and 20°C as surface temperature) necessary for TSR, the calcium sulfate enriched in pore water will react with hydrocarbons to form H_2S and CO_2. TSR will continue to the maximum burial of about 5000 m, equivalent to the temperature of 200°C. Calcite and dolomite are interpreted to be formed in late-diagenetic stage based on the petrographic and geochemical evidence investigated in this study (Figures 9(e) and 9(f)). The spatial distribution of calcite, along with that of secondary dolomite, authigenic quartz, and pyrite, in combination with carbon and oxygen data further indicates that the calcite in anhydrite dissolution pores is genetically related to thermochemical sulfate reduction.

In contrast to the southeastern Ordos Basin, the Jingbian Gas Field is located in the tectonic high in paleogeography, and the anhydrite dissolution water after leaching by meteoric water is taken away from its open system, leaving the molds open (Figure 9(e)). The sea water flooded in the southeastern direction has not emerged within the Jingbian region. The TSR reaction rarely occurs for the lack of dissolved sulfate in the pore water. Although some molds are also filled with minerals in the Jingbian Gas Field, the filling degree is much lower than that in the southeastern Ordos Basin (Figure 2). Therefore, the resultant porosity in the mold is preserved resulting in the high porosity and permeability of the Jingbian Gas Field (Figures 2 and 3).

6. Conclusions

The anhydrite nodule-bearing dolomite is widely distributed in the upper Majiagou Formation of the southeastern Ordos Basin. Nevertheless, the anhydrite dissolution pores are commonly filled by minerals such as dolomite, calcite, pyrite, and quartz, which resulted in significant porosity and volume reduction. The calcite filling in anhydrite dissolution pores is interpreted to be precipitated as TSR by-product, which is supported by its relatively negative $\delta^{18}O$ value (-15.58‰ ~-8.96‰ VPDB) and negative $\delta^{13}C$ value (-7.56‰~0.26‰ VPDB). The higher homogenization temperatures (140-234°C) and high salinity (19.13-23.18 wt.% NaCl equivalent) of the primary inclusions in calcite confirm the above interpretation. Dolomite is the second most abundant carbonate formed as a by-product of TSR, which is promoted by the precipitation of calcite and resulted enriched in Mg^{2+}/Ca^{2+} ratio in the pore water. Pyrite forms by the reaction of H_2S released from TSR with the Fe^{2+} in the horizon, which is supported by its cubic habit and relatively high $\delta^{34}S$ value (10.50‰~24.00‰). Quartz with relatively high homogenization temperature (113-154°C) is considered to precipitate in low-pH solution from calcite and pyrite precipitation after TSR.

The paleogeographic location of the southeastern Ordos Basin is much lower than that of the Jingbian Gas Field, which is submerged in the sea water of marine phreatic environments for a long time when sea water flooded from the

southeastern direction. Owing to the periodic sea-level changes, the connate marine pore water is altered locally by minor amounts of evaporative water during shallow burial resulted in the pore water enriched in calcium sulfate. The Jingbian Gas Field, however, is located in the tectonic high in paleogeography which has not been emerged by sea water. TSR rarely occurs for the lack of enriched pore water. Therefore, the resultant porosity in the nodule is preserved and rarely filled by other minerals resulting in the high porosity and permeability of the Jingbian Gas Field.

Data Availability

The data presented in this study are available on request from the corresponding author.

Conflicts of Interest

The authors declare no conflict of interest.

Authors' Contributions

Conceptualization, methodology, and writing of original draft were done by Lihong Liu. Investigation and writing (review and editing) were done by Chunlian Wang. Resources and funding were acquired by Zhili Du. Validation, visualization, and project administration were done by Jianghua Gong. All authors have read and agreed to the published version of the manuscript.

Acknowledgments

This work is supported by the National Natural Science Foundation of China (No. 41802173), Central Welfare Basic Scientific Research Business Expenses (No. KK2005), and China Geological Survey projects ((Nos. DD20160175, DD20190106, DD20190708, DD20190090, and DD20190606). The work is part of the outcome of the first author's PhD thesis (Peking University), under the guidance of Prof. Yongsheng Ma (Sinopec Co., Ltd.) and Prof. Bo Liu (Peking University), who are greatly acknowledged. We are grateful to Dr. Xuefeng Zhang for his constructive comments and suggestions that have significantly improved the manuscript. We would like to thank Hongguang Liu and Qicai Jiang of Peking University for picking minerals in the pores in dealing with samples. We heartily thank all those involved in the field study.

References

[1] T. M. Chowns and J. E. Elkins, "The origin of quartz geodes and cauliflower cherts through the silicification of anhydrite nodules," *SEPM Journal of Sedimentary Research*, vol. 44, pp. 885–903, 1974.

[2] M. A. Bustillo, J. Garcia-Guinea, J. Martinez-Frias, and A. Delgado, "Unusual sedimentary geodes filled by gold-bearing hematite laths," *Geological Magazine*, vol. 136, no. 6, pp. 671–679, 1999.

[3] J. H. Geeslin and H. S. Chafetz, "Ordovician Aleman Ribbon Cherts: an example of silicification prior to carbonate lithification," *SEPM Journal of Sedimentary Research*, vol. 52, pp. 1283–1293, 1982.

[4] R. G. Maliva, "Quartz geodes: early diagenetic silicified anhydrite nodules related to dolomitization," *SEPM Journal of Sedimentary Research*, vol. 57, pp. 1054–1059, 1987.

[5] H. P. Bao, C. Y. Yang, and J. S. Huang, ""Evaporation drying" and"reinfluxing and redissolving"—a new hypothesis concerning formation of the Ordovician evaporites in eastern Ordos Basin," *Journal of Palaeogeography*, vol. 6, pp. 279–288, 2004.

[6] Z. X. He, *The Evolution and Petroleum of Ordos Basin*, Petroleum Iindustry Press, Beijing, 2003.

[7] C. Pierre and J. M. Rouchy, "Carbonate replacements after Sulfate evaporites in the Middle Miocene of Egypt," *SEPM Journal of Sedimentary Research*, vol. 58, pp. 446–456, 1988.

[8] J. Peckmann, J. Paul, and V. Thiel, "Bacterially mediated formation of diagenetic aragonite and native sulfur in Zechstein carbonates (Upper Permian, Central Germany)," *Sedimentary Geology*, vol. 126, no. 1-4, pp. 205–222, 1999.

[9] A. C. Kendall, "Late diagenetic calcitization of anhydrite from the Mississippian of Saskatchewan, western Canada," *Sedimentology*, vol. 48, no. 1, pp. 29–55, 2001.

[10] J. K. Warren, *Evaporites: Sediments, Resources and Hydrocarbons*, Springer, Berlin, 2006.

[11] D. S. Ulmer-Scholle and P. A. Scholle, "Replacement of evaporites within the Permian Park City Formation, Bighorn Basin, Wyoming, USA," *Sedimentology*, vol. 41, no. 6, pp. 1203–1222, 1994.

[12] C. Cai, W. Hu, and R. H. Worden, "Thermochemical sulphate reduction in Cambro-Ordovician carbonates in Central Tarim," *Marine and Petroleum Geology*, vol. 18, no. 6, pp. 729–741, 2001.

[13] M. Harwoodg, "Calcitized anhydrite and associated sulphides in the English Zechstein First Cycle Carbonate (EZ1 Ca)," in *The Zechstein Basin with Emphasis on Carbonate Sequences. Contributions to Sedimentology 91*, H. Fiichtbauer and T. M. Peryt, Eds., pp. 61–72, E. Schweizerbart'sche Verlagsbuchhandlung (Nagele u. Obermiller), Stuttgart, 1980.

[14] M. R. Lee and G. M. Harwood, "Dolomite calcitization and cement zonation related to uplift of the Raisby Formation (Zechstein carbonate), northeast England," *Sedimentary Geology*, vol. 65, no. 3-4, pp. 285–305, 1989.

[15] P. A. Scholle, D. S. Ulmer, and L. A. Melim, "Late-stage calcites in the Permian Capitan Formation and its equivalents, Delaware Basin margin, West Texas and New Mexico: evidence for replacement of precursor evaporites," *Sedimentology*, vol. 39, no. 2, pp. 207–234, 1992.

[16] H. Yang, J. H. Fu, X. S. Wei, and J. F. Ren, "Natural gas exploration domains in Ordovician marine carbonates, Ordos Basin," *Acta Petrolei Sinica*, vol. 32, pp. 733–740, 2011.

[17] Z. Z. Feng, Z. D. Bao, and Q. F. Kang, "Palaeotectonics of Ordovician in Ordos," *Journal of Palaeogeography*, vol. 1, pp. 83–94, 1999.

[18] J. H. Fu and C. B. Zhen, "Evolution between North China Sea and Qilian Sea of the Ordovician and the characteristics of lithofacies palaeogeography in Ordos Basin," *Journal of Palaeogeography*, vol. 3, pp. 25–34, 2001.

[19] X. S. Wei, J. F. Ren, J. X. Zhao et al., "Paleo-geomorphologic characteristic evolution and geological significance of the Ordovician weathering crust in eastern Ordos Basin," *Acta Petrolei Sinica*, vol. 38, pp. 999–1009, 2017.

[20] Z. T. Su, H. D. Chen, Z. J. Ouyang, and X. Q. Jin, "Sequence-based lithofacies and paleogeography of Majiagou formation in Ordos Basin," *Geology in China*, vol. 39, pp. 623–633, 2012.

[21] Z. H. Li and J. M. Hu, "Characteristics of holes filling in Ordovician of Ordos Basin," *Geological Review*, vol. 57, pp. 444–456, 2011.

[22] J. F. Ren, H. P. Bao, L. Y. Sun, and B. X. Liu, "Characteristics and mechanism of pore-space filling of Ordovician Weathering crust karst reservoirs in Ordos Basin," *Marine Petroleum Geology*, vol. 17, pp. 63–69, 2012.

[23] J. Hoefs, *Stable Isotope Geochemistry*, Springer, Berlin, 2009.

[24] A. M. Alonso-Zarza, Y. Sánchez-Moya, M. A. Bustillo, A. Sopeña, and A. Delgado, "Silicification and dolomitization of anhydrite nodules in argillaceous terrestrial deposits: an example of meteoric-dominated diagenesis from the Triassic of Central Spain," *Sedimentology*, vol. 49, no. 2, pp. 303–317, 2002.

[25] G. Chi, L. W. Diamond, H. Lu, J. Lai, and H. Chu, "Common problems and pitfalls in fluid inclusion study: a review and discussion," *Minerals*, vol. 11, no. 1, p. 7, 2021.

[26] H. Bao, F. Yang, Z. Cai, Q. Wang, and C. Wu, "Origin and reservoir characteristics of Ordovician dolostones in the Ordos Basin," *Natural Gas Industry*, vol. 4, no. 2, pp. 106–119, 2017.

[27] F. Zengzhao, Z. Yongsheng, and J. Zhenkui, "Type, origin, and reservoir characteristics of dolostones of the Ordovician Majiagou Group, Ordos, North China Platform," *Sedimentary Geology*, vol. 118, no. 1-4, pp. 127–140, 1998.

[28] B. Q. Wang and I. S. Al-Aasm, "Karst-controlled diagenesis and reservoir development; example from the Ordovician mainreservoir carbonate rocks on the eastern margin of the Ordos basin, China," *AAPG Bulletin*, vol. 86, pp. 1639–1658, 2002.

[29] H. R. Qing, G. Chi, and S. Zhang, "Origin of coarse-crystalline calcite cement in Early Ordovician carbonate rocks, Ordos basin, northern China: Insights from oxygen and carbon isotopes and fluid inclusion microthermometry," *Journal of Geochemical Exploration*, vol. 89, no. 1-3, pp. 344–347, 2006.

[30] L. Jiang, W. Pan, C. Cai et al., "Fluid mixing induced by hydrothermal activity in the Ordovician carbonates in Tarim Basin, China," *Geofluids*, vol. 15, no. 3, 498 pages, 2015.

[31] L. A. Hardie, "Dolomitization; a critical view of some current views," *Journal of Sedimentary Research*, vol. 57, no. 1, pp. 166–183, 1987.

[32] P. W. Choquette and N. P. James, "Limestones-burial diagenetic environments," in *Diagenesis*, I. A. Mcilreath and D. W. Morrow, Eds., vol. 4, pp. 75–112, Geosci. Can. Reprint Ser., 1990.

[33] L. H. Liu, Y. S. Ma, B. Liu, and C. L. Wang, "Hydrothermal dissolution of Ordovician carbonates rocks and its dissolution mechanism in Tarim Basin, China," *Carbonates and Evaporites*, vol. 32, no. 4, pp. 525–537, 2017.

[34] R. H. Worden and P. C. Smalley, "H_2S-producing reactions in deep carbonate gas reservoirs: Khuff Formation, Abu Dhabi," *Chemical Geology*, vol. 133, no. 1-4, pp. 157–171, 1996.

[35] H. Irwin, C. Curtis, and M. Coleman, "Isotopic evidence for source of diagenetic carbonates formed during burial of organic-rich sediments," *Nature*, vol. 269, no. 5625, pp. 209–213, 1977.

[36] L. Jia, C. Cai, H. Yang et al., "Thermochemical and bacterial sulfate reduction in the Cambrian and Lower Ordovician carbonates in the Tazhong Area, Tarim Basin, NW China: evidence from fluid inclusions, C, S, and Sr isotopic data," *Geofluids*, vol. 15, no. 3, 437 pages, 2015.

[37] H. G. Machel, "Gas souring by thermochemical sulfate reduction at 140°C: discussion," *American Association of Petroleum Geologists Bulletin*, vol. 82, pp. 1870–1873, 1998.

[38] H. G. Machel, "Bacterial and thermochemical sulfate reduction in diagenetic settings – old and new insights," *Sedimentary Geology*, vol. 140, no. 1-2, pp. 143–175, 2001.

[39] Z. L. Ren, Q. Yu, J. P. Cui et al., "Thermal history and its controls on oil and gas of the Ordos Basin," *Earth Science Frontiers*, vol. 24, pp. 137–148, 2017.

[40] D. Zhu, Q. Meng, Z. Jin, and W. Hu, "Fluid environment for preservation of pore spaces in a deep dolomite reservoir," *Geofluids*, vol. 15, no. 4, 545 pages, 2015.

[41] K. Christof, O. Marcus, and A. G. Sarah, "Partitioning of arsenic between hydrothermal fluid and pyrite during experimental siderite replacement," *Chemical Geology*, vol. 500, pp. 136–147, 2018.

[42] S. Lubna, H. Itay, S. Ward et al., "Dynamics of pyrite formation and organic matter sulfurization in organic-rich carbonate sediments," *Geochimica et Cosmochimica Acta*, vol. 241, pp. 219–239, 2018.

[43] N. Wang, "The advances in the study of microbial dolomite," *Acta Petrologica et Mineralogica*, vol. 30, pp. 690–783, 2011.

[44] X. Zhang, Y. F. Zhou, and T. H. Chen, "An experimental study of the decomposition of gypsum as the function of contacted sulfate reducing bacterium and its metabolites," *Acta Petrologica et Min-Eralogica*, vol. 34, pp. 932–938, 2015.

[45] X. J. Meng, Z. Q. Hou, and Z. Q. Li, "Sulfur and lead isotope compositionsof the Qulong porphyry copper deposit, TiBet: implications for the sources of plutons and metals in the deposit," *Acta Geologica Sinica*, vol. 80, pp. 554–560, 2006.

[46] C. Pierre, J. M. Rouchy, and A. Gaudichet, "Diagenesis in the gas hydrate sediments of Blake Ridge: mineralogy and stable isotope compositions of the carbonate and sulfide minerals," in *proceedings of the ocean drilling program*, C. K. Paull, R. Matsumoto, and P. J. Wallace, Eds., vol. 164, pp. 139–146, Scientific Results, 2000.

[47] Z. Liu, D. Chen, J. Zhang et al., "Pyrite morphology as an Indicator of Paleoredox conditions and shale gas content of the Longmaxi and Wufeng Shales in the Middle Yangtze Area, South China," *Minerals*, vol. 9, no. 7, p. 428, 2019.

[48] J. R. Postgate, *The Sulfate-reducing Bacteria*, Cambridge University Press, Cambridge, 2nd edition, 1984.

[49] H. L. Ehrlich, *Geomicrobiology*, Marcel Dekker, New York, 2nd edition, 1990.

[50] Q. Liu, D. Zhu, Z. Jin, C. Liu, D. Zhang, and Z. He, "Coupled alteration of hydrothermal fluids and thermal sulfate reduction (TSR) in ancient dolomite reservoirs - an example from Sinian Dengying Formation in Sichuan Basin, southern China," *Precambrian Research*, vol. 285, pp. 39–57, 2016.

[51] Y. S. Ma, S. Zhang, T. Guo, G. Zhu, X. Cai, and M. Li, "Petroleum geology of the Puguang sour gas field in the Sichuan Basin, SW China," *Marine and Petroleum Geology*, vol. 25, no. 4-5, pp. 357–370, 2008.

[52] K. K. Li, C. Cai, D. Hou et al., "Origin of high H_2S concentrations in the Upper Permian Changxing reservoirs of the Northeast Sichuan Basin, China," *Marine and Petroleum Geology*, vol. 57, pp. 233–243, 2014.

[53] J. Ganor, T. J. Huston, and L. M. Walter, "Quartz precipitation kinetics at 180°C in NaCl solutions–implications for the

usability of the principle of detailed balancing," *Geochimica et Cosmochimica Acta*, vol. 69, no. 8, pp. 2043–2056, 2005.

[54] R. Wierzbicki, J. J. Dravis, I. al-Aasm, and N. Harland, "Burial dolomitization and dissolution of upper Jurassic Abenaki platform carbonates, deep Panuke reservoir, Nova Scotia, Canada," *AAPG Bulletin*, vol. 90, no. 11, pp. 1843–1861, 2006.

[55] F. Hao, X. Zhang, C. Wang et al., "The fate of CO_2 derived from thermochemical sulfate reduction (TSR) and effect of TSR on carbonate porosity and permeability, Sichuan Basin, China," *Earth-Science Reviews*, vol. 141, pp. 154–177, 2015.

[56] Z. T. Su, H. D. Chen, J. X. Zhao, J. Li, Q. Xu, and X. Gao, "Difference analysis of palaeokarst development in middle and south parts of Ordos Basin," *Fault-Block Oil & Gas Field*, vol. 17, pp. 542–547, 2010.

[57] J. S. Archer and C. G. Wall, *Petroleum Engineering Principles and Practice*, Graham & Trotman, London, 1986.

[58] A. C. Lasaga and R. J. Kirkpatrick, "Kinetics of geochemical processes," *Mineral. Soc. Am., Rev. Mineral*, vol. 8, p. 398, 1981.